



Study on fluoride evaporation from casting powders

Elena Brandaleze¹ · Marcelo Valentini¹ · Leandro Santini¹ · Edgardo Benavidez¹

Received: 7 August 2017 / Accepted: 27 March 2018 / Published online: 7 April 2018
© Akadémiai Kiadó, Budapest, Hungary 2018

Abstract

Casting powders are commonly used in continuous casting of steels. The chemical composition of these powders is based on various oxides, carbonaceous materials and fluoride compounds. The purpose of fluorite (CaF_2) addition is to control viscosity, fluidity temperature and cuspidine crystallization during casting. Unfortunately, fluoride compounds are lost in the vapour phase during the casting operations, due to the high vapour pressure of these compounds. In view of the environmental problems associated with the evaporation of fluoride from the casting powders, a kinetic study on the fluoride evaporation was carried out. Three commercial casting powders with different fluoride contents (between 2.6 and 10.6 mass%) were selected in this study. Powders characterization includes the melting behaviour determined by hot stage microscopy, the physical properties such as viscosity estimated by Fact Sage 7.1 and surface tension calculated on the base of contact angle measurements. The crystallization tendency of the samples was determined by microscopy observations on samples quenched from 1300 °C. The emission study includes thermal analysis (DTA–TG) tests. The different phases present in the system were predicted through thermodynamic simulation. The gaseous species predicted were: NaF, KF, $(\text{NaF})_2$, NaAlF_4 , KAlF_4 and SiF_4 . It was possible to establish that the fluoride gases emissions occur when the samples present liquid phases. The type of fluoride gas is determined by the chemical composition of the casting powders, while the percentage of emissions depends on both the viscosity and surface tension of liquids.

Keywords Continuous casting · Casting powders · Thermal analysis · Kinetics · Fluorine emissions

Introduction

Casting powders (or mould powders) play important roles in the continuous casting of steel, such as protecting the molten steel from oxidation, absorbing inclusions, providing thermal insulation, lubricating the strand and controlling heat transfer between the mould and the steel shell. All these functions are mainly controlled by the chemical composition, physical properties such as viscosity, surface tension and crystallization tendency. The chemical composition of the casting powders is based on various oxides, carbonaceous materials and fluoride compounds such as fluorite (CaF_2) to control the viscosity, fluidity and crystallization of these materials during the process [1]. These

properties are essential to predict the lubrication and heat transfer performances of casting powders in the continuous casting process.

The purpose of adding fluorite (CaF_2) up to 10 or 12 mass% is to decrease the slag viscosity, to decrease the liquidus temperature and to increase the precipitation of cuspidine ($\text{Ca}_4\text{Si}_2\text{O}_7\text{F}_2$) at the mould-strand gap. Unfortunately, during the steel casting operations, fluorides compounds promote the formation of gaseous phases, by reaction among with the CaF_2 and some of the species present in the slag. In addition, humidity in the flux can react with CaF_2 resulting in the formation of HF. The gases emissions tend to cause many problems, such as environmental pollution (contamination of cooling water and the atmosphere), corrosion of casting facilities and health problems to the operators [2, 3]. For this reason, it is necessary to increase the knowledge on the kinetic of fluorides evaporation from casting powders at continuous casting conditions.

Currently, global demand for steel products is constantly increasing. Therefore, it is necessary to have a better

✉ Elena Brandaleze
ebrandaleze@frsn.utn.edu.ar

¹ Department of Metallurgy and Center DEYTEMA, Facultad Regional San Nicolás, Universidad Tecnológica Nacional, Colón 332, B2900LWH San Nicolás, Argentina

understanding of steel production and its relation to sustainable development, human health and the environment. In spite of its industrial importance, the phase equilibrium of fluorine contained in oxide systems has not been well investigated due to the complexity of their chemistry and the difficulties in performing experiments [4]. Thus, no systematic thermodynamic modelling of these systems has been conducted to date.

Persson et al. [2] inform that fluorine and alkaline emissions, produced during the casting process, cause variations in the viscosity values due to changes in the chemical composition of the casting powders. Sasaki et al. [5] comment that the partial substitution of fluorine anions for oxygen in molten silicates and aluminosilicates shows drastic effects on physical properties, such as the fluidity (as the inverse of viscosity) and the melting point of systems. They provide important structural information determined by Raman spectroscopy. Tian et al. [6] confirm that the surface tension of the glassy phases determines the growth of the bubbles in the molten glass, and this factor is relevant for the gases emissions. The stability of some systems which present different oxides was also studied by different researchers such as Wang [7] and Mills [8]. The crystallization tendency is an important factor to control the heat transfer in the mould gap. The main crystalline phase generated at process conditions is cuspidine ($3\text{CaO}\cdot 2\text{SiO}_2\cdot \text{CaF}_2$) which presents fluorine in its chemical composition.

In this work, the kinetics of fluorides emissions was studied by DTA–TG tests, performed on three commercial casting powders with different fluorite contents. These results were correlated with both information obtained through the thermodynamic simulation and physical properties determined at different temperatures. In order to know the melting behaviour of these powders, three critical temperatures: T_S (softening temperature), T_H (hemisphere temperature) and T_F (fluidity temperature) were determined by hot stage microscopy (HSM). The viscosity was estimated by thermodynamic simulation using the software FactSage 7.1. The surface tension is calculated on the base of the contact angle measurements carried out by HSM on all the casting powders selected in order to justify the gas emissions. The crystallization tendency and other structural aspects were studied in this paper by different microscopy techniques: light and scanning electron microscopy (SEM) with EDS analysis. Gases, liquid and solid phases were also identified by thermodynamic simulation of the system at different temperatures. It was possible to corroborate that the fluoride evaporation occurs when the mould fluxes present one or more liquid phases during the melting of the casting powder. It is important to note that during the last years, large thermodynamic databases of multicomponent oxides systems have been developed and parameters have

been optimized in order to reproduce all reliable experimental data within experimental errors [9, 10]. The information obtained through FactSage 7.1 in this study presents a valuable contribution in order to understand the complex systems associated with the casting powders at process conditions. The structural observations analysed by SEM–EDS allow corroborating results obtained by thermodynamic predictions.

Methodology

In this paper, the emissions study includes results of DTA–TG integrated with thermodynamic simulation that provides useful information, at a certain temperature, about phases (gas, liquid and solid) present in the system (including their chemical composition). The present work consists of two parts: (a) the characterization of the casting powders samples and (b) the study of the emissions produced by these powders at continuous casting conditions.

The chemical composition of casting powders was determined combining X-Ray fluorescence (XRF) and wet techniques.

The melting behaviour of samples was analysed by hot stage microscopy test (HSM) determining the critical temperatures: T_S (softening temperature), T_H (hemisphere temperature) and T_F (fluidity temperature). Samples used in HSM tests were cylindrical compacts 5 mm in diameter and 5 mm in height. Heating rates of $5\text{ }^\circ\text{C min}^{-1}$ were employed in all HSM runs.

Using the HSM images, the contact angle was determined. The surface tension was estimated by mathematical calculus on the base of the contact angle measurements.

The viscosity of the different liquids was estimated at different temperatures applying FactSage 7.1, considering the viscosity module and the glass option.

The crystallization tendency and the characterization of the crystalline and glassy phases were carried out by optical microscopy using an Olympus GX51 microscope (with image analysis system Leco IA 32), and by scanning electronic microscopy (SEM) using a FEI QUANTA 200F equipment (with EDS). Samples were included in resin and polished with SiC papers from 320 to 1000 grit, then with diamond paste from 6 to $1\text{ }\mu\text{m}$ and the final polishing was carried out with Al_2O_3 (particle size of $0.03\text{ }\mu\text{m}$) suspended in distilled water, in Vibromet vibratory polisher. The SEM–EDS analysis allowed to corroborate the results obtained by thermodynamic predictions.

The study of casting powder emissions was performed by differential thermal analysis and thermogravimetry (DTA/TG) up to $1450\text{ }^\circ\text{C}$ in air using a SHIMADZU DTG-60/60H instrument, at a heating rate of $10\text{ }^\circ\text{C min}^{-1}$. Samples of 10 mg were tested in powder form in alumina

crucible without purge gas. A similar mass of Al_2O_3 (10 mg) was used as reference material.

Experimental results were correlated with those obtained from Fact Sage 7.1 simulations. In this case, the Equilib module and the databases FToxid and FTmis were employed.

Results and discussion

Three commercial casting powders (named A, B and C) with different content of fluorite (CaF_2) and CaO/SiO_2 ratio (basicity index BI) were selected in this study. The percentage (mass%) of oxides and CaF_2 present in these materials are shown in Table 1.

According to Table 1, the range of CaF_2 was 2.6–10.2 mass%, and the basicity CaO/SiO_2 : 0.70–0.87.

The casting powders in the industry are selected according to the steel grade, the type of product (slabs, billets, etc.) and the casting process conditions (casting rate, cooling capacity, etc.) [1]. In practice, powders A and B are applied for low and medium carbon steel slab production, while powder C is applied in steel billet casting.

Casting powders characterization

The melting behaviour of the samples was determined by HSM tests. The results are described by three critical temperatures: T_S , T_H and T_F . In Table 2 are listed the critical temperatures determined from the melting range of casting powders.

The softening temperature (T_S) is considered the point at which the formation of liquid phases begins. As an example, Fig. 1 shows typical images corresponding to critical temperatures of sample C. In all runs, the initial temperature (indicated as T_I) was 20 °C.

From Table 2, it is observed that the samples A and B (used for low and medium carbon steels) present the lowest critical temperatures and in consequence present liquid phases at a lower temperature range than sample C. During casting of steel, long products (such as billets) casting powders with high critical temperatures such as those shown in sample C are used [1].

The surface tension (γ) during melting was established on the base of the contact angle (θ) measurements and mathematical calculus from the Eq. 1 [11]:

Table 2 Critical temperatures of casting powders and surface tension estimated at T_F

| Powder | $T_S/^\circ\text{C}$ | $T_H/^\circ\text{C}$ | $T_F/^\circ\text{C}$ | $\gamma/\text{mN/m}$ |
|--------|----------------------|----------------------|----------------------|----------------------|
| A | 1072 | 1091 | 1134 | 195 |
| B | 1077 | 1094 | 1130 | 194 |
| C | 1174 | 1187 | 1255 | 203 |

$$\gamma = \frac{h^2 \cdot \rho \cdot g}{2 \cdot (1 - \cos \theta)} \quad (1)$$

where h is the height of drop (in m), ρ is the density of melt (in kg m^{-3}) and g is the acceleration of gravity (in m s^{-2}). The values of surface tension (in mN m^{-1}) estimated at the fluidity temperature of each casting powders are listed in Table 2. The density of the liquid mould slag is calculated from partial molar volumes ($V = M/\rho$ where M = molecular weight) as shown in Eqs. 2, 3 and 4 according to Mills [12]:

$$V_{1773} = \sum_{i=1}^N (X_i V_i) \quad (2)$$

$$V_T = V_{1773} + 0.001 (T - 1773 \text{ K}) \quad (3)$$

$$V_T = M/\rho_T \quad (4)$$

Samples A and B present the lowest values of surface tension at T_F (fluidity temperature). The highest γ value in the sample C is justified by the impact of the Al_2O_3 content (14.4 mass%). The influence of Al_2O_3 addition on the surface tension of high alkali aluminosilicate glasses ($\text{SiO}_2\text{-Al}_2\text{O}_3\text{-RO-R}_2\text{O}$) was studied by Tian et al. [6]. They concluded that the surface tension of these glasses increased approximately linearly when Al_2O_3 content increased from 5 to 20 mass%.

The viscosity, estimated by FactSage simulation, at the temperature range between 1300 and 1400 °C is plotted in Fig. 2. The highest viscosity is obtained for the sample C (used in billet casting). It is observed that the lowest viscosity values are determined for the samples A and B. It is important to note that the higher content of CaF_2 in casting powders promotes lower values of melting temperatures, surface tension and viscosity. These results are consistent with those informed by Mills [8].

Table 1 Chemical composition of the casting powders

| Powder | BI | SiO_2 | Al_2O_3 | CaO | MgO | MnO | Na_2O | K_2O | TiO_2 | B_2O_3 | Fe_2O_3 | CaF_2 | P_2O_5 |
|--------|------|----------------|-------------------------|------|-----|------|-----------------------|----------------------|----------------|------------------------|-------------------------|----------------|------------------------|
| A | 0.87 | 36.5 | 5.0 | 31.8 | 1.5 | – | 12.3 | 0.6 | – | 0.3 | 1.4 | 10.2 | – |
| B | 0.81 | 33.7 | 2.4 | 27.4 | 1.6 | 0.05 | 11.3 | 0.5 | – | – | 1.6 | 9.0 | 0.4 |
| C | 0.70 | 31.6 | 14.4 | 22.2 | 2.1 | 0.30 | – | 1.6 | 1.0 | – | 3.4 | 2.6 | 0.5 |

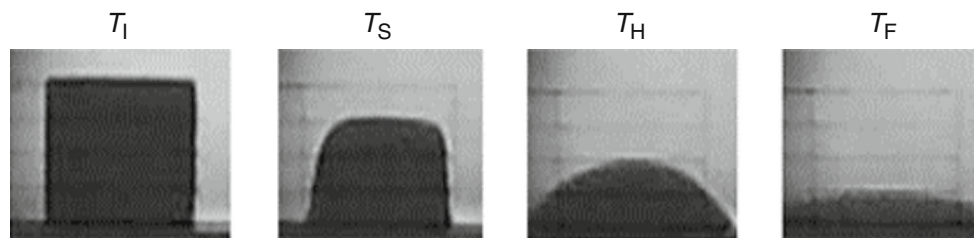


Fig. 1 HSM images at critical temperatures corresponding to sample C

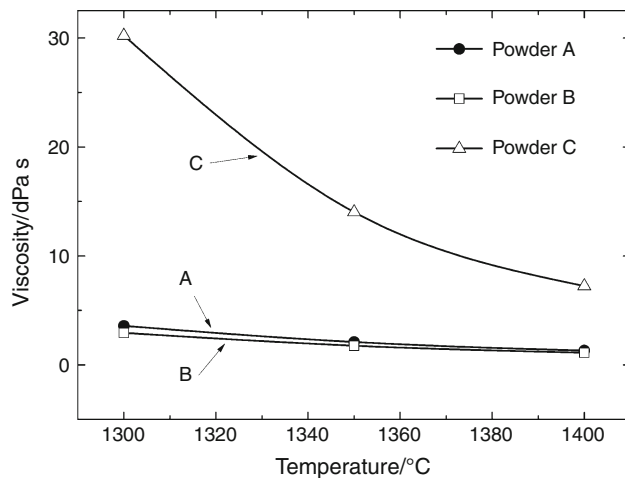


Fig. 2 Viscosity estimation of casting powders applying FactSage

Other important factor in the continuous casting is the crystallization tendency of casting powders, because it affects the heat transfer in the mould and could produce cracks in the steel product [13]. The surface cracking of continuously cast steel has drawn the attention and focus of many researchers, since it affects the efficiency of the casting process [13].

The structural characteristic was evaluated on samples quenched from 1300 °C. Figure 3 presents images of the samples with the highest and lowest contents of CaF_2 , sample A (10.2%) and C (2.6%), respectively. In Fig. 3a is

observed a crystalline layer formed at the surface of the quenched sample A, while in sample C no crystalline phases were observed (Fig. 3b).

The study shows that samples A and B present a thin surface layer of crystals, such as the observed in Fig. 3a. By EDS, it was possible to identify cuspidine ($3\text{CaO}\cdot 2\text{SiO}_2\cdot \text{CaF}_2$) as the main crystalline phase presents in both samples (A and B). Cuspidine is the characteristic crystalline phase present during cooling of mould powders containing fluorine [14]. This information is consistent with those informed in [4] and it was corroborated by thermodynamic simulation of these systems (samples A and B) at the same temperature conditions. The presence of cuspidine demonstrates that part of fluorine is retained in the material in a solid crystalline phase.

On the other hand, sample C is fully glassy. The pores observed in different zones of quenched samples confirm the gaseous emissions from the melted casting powders at 1300 °C.

Casting powders emissions

In order to evaluate the percentage of mass loss and the phase transformations present in the powders, at the temperature range: 900–1300 °C, the DTA and TG curves were considered. These curves are visualized in Figs. 4–6. The gas phases identified for each sample are indicated in the curves associated with the emission temperature.

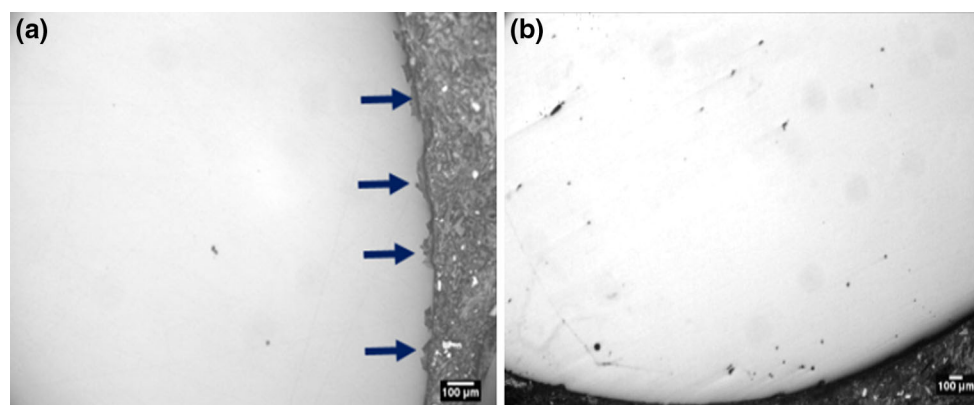


Fig. 3 Structural aspect of the samples quenched from 1300 °C: a powder A and b powder C

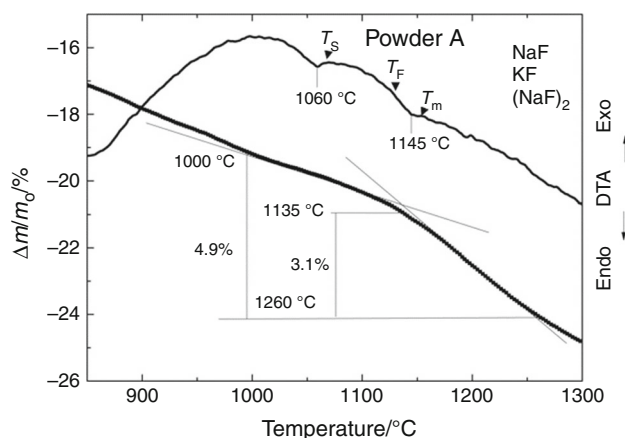


Fig. 4 DTA/TG curves with gases emissions detail of casting powder A

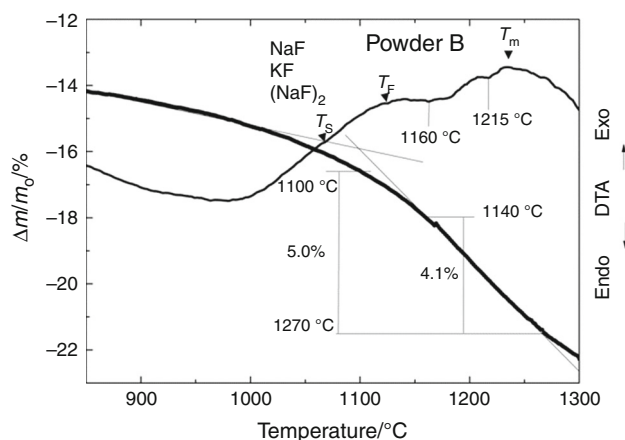


Fig. 5 DTA/TG curves with gases emissions detail of casting powder B

From the chemical compositions, the viscosity at 1400 °C of the liquids present in sample A (L_{1A} and L_{2A}), sample B (L_{1B}) and sample C (L_{1C} and L_{2C}) was estimated applying FactSage (module: MELTS). The values of η (in dPa s) are listed in Table 3.

Figures 4–6 show that at lower temperatures the main mass losses are produced by humidity loss (up to ≈ 200 °C), and decompositions of carbonaceous materials and carbonates (between 400 and 850 °C).

Table 3 Viscosities of liquids present at 1400 °C

| Liquid | η /dPa s |
|----------|---------------|
| L_{1A} | 1.1 |
| L_{2A} | 0.2 |
| L_{1B} | 2.4 |
| L_{1C} | 18 |
| L_{2C} | 25 |

Figure 4 shows TG and DTA curves of sample A, containing 10.2% CaF_2 and NaO_2 (12.3 mass%), K_2O (0.6 mass%) and B_2O_3 (0.3 mass%).

Fluoride gases emissions in all the samples start from ≈ 1000 °C, when the melting of the sample starts and the first liquid phases are present in the system. Table 4 shows a comparison between the fluidity temperatures of the samples, obtained through HSM and DTA tests. It is relevant to mention that HSM test does not determine the melting point. However, the fluidity temperatures obtained by both methods are consistent.

In sample A, two liquid phases are predicted in the system at 1000 °C: L_{1A} and L_{2A} . At this temperature, volatile species NaF, KF and $(\text{NaF})_2$ are predicted. The results obtained by DTA–TG are consistent with the melting behaviour of the sample determined by HSM. The emissions finished at ≈ 1400 °C. On the base of the chemical composition of the liquids L_{1A} and L_{2A} (at 1400 °C), it was possible to estimate the viscosity of both: (L_{1A}) = 1.1 dPa s and (L_{2A}) = 0.2 dPa s. Namely, both liquids have relative low viscosity.

The curve indicates that the mass loss between 1130 and 1300 °C is $\Delta m/m_0 = 3.1\%$.

Two powerful surfactants are present in both liquid phases: CaF_2 and B_2O_3 , justifying the lowest surface tension obtained in sample A at T_F (≈ 1130 °C). Namely, these surfactants promote the sodium and potassium fluorine gases emissions from the liquid phases (L_{1A} and L_{2A}). One part of the F^- ions is trapped in the cuspidine crystalline phase (present in the surface crystal layer observed by optical microscopy) and the rest remains in the glassy phase as it is mentioned by Zhou et al. [15]. By FactSage, which uses a Gibbs energy minimization routine, the solid phases were corroborated.

Similar phenomena were found in sample B (9.0% CaF_2 and contents of $\text{NaO}_2 = 11.3\%$, and $\text{K}_2\text{O} = 0.5\%$). This sample also presents a mass loss ($\Delta m/m_0 = 4.1\%$) between 1140 and 1270 °C (Fig. 5). The main fluorine gases emissions start from ≈ 1140 °C when the liquid phase L_{1B} is formed in this system (consistent with the fluidity temperature determined by HSM). Gaseous species: NaF, KF and $(\text{NaF})_2$, similar to those predicted to sample A are expected. The estimated viscosity of this liquid at 1400 °C

Table 4 Comparison between the fluidity temperatures obtained by HSM and by DTA

| Powder | T_F /°C (HSM) | T_F /°C (DTA) |
|--------|-----------------|-----------------|
| A | 1134 | 1130 |
| B | 1130 | 1127 |
| C | 1255 | 1254 |

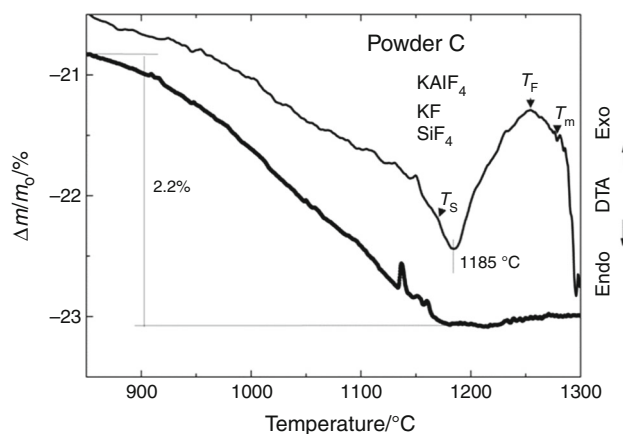


Fig. 6 DTA/TG curves with gases emissions detail of casting powder C

is (L_{1B}) = 2.4 dPa s. Although this liquid presents a slightly higher viscosity than the liquids of sample A, it is observed that the surface tension of sample B (determined by L_{1B}) at the fluidity temperature is similar to that of sample A at T_F (determined by L_{1A} and L_{2A}). Thus, the low surface tension can be taking an important role in the kinetic of gaseous emissions, as discussed below.

Finally, the sample C, with 2.6 mass% CaF_2 and low content of K_2O (1.6 mass%), presents a total mass loss $\Delta m/m_0 = 2.2\%$ between 900 and 1200 °C. At higher temperatures than 1200 °C, no mass losses were detected. The main gases emissions of this sample are produced in the temperature range 1100–1200 °C, and the gaseous species include: KAlF_4 , KF and SiF_4 because the powder do not contain Na_2O . Two liquid phases are predicted in this system: L_{1C} and L_{2C} , with high viscosity in both cases: $\eta(L_{1C}) = 18$ dPa s., $\eta(L_{2C}) = 25$ dPa s. In this case, both high viscosity liquids with high surface tension at melting temperatures are present in sample C.

The results obtained show that the chemical composition of casting powders determines the type of gases emissions produced. However, the percentage of emissions is controlled by the viscosity and the surface tension (determined by type and content of surfactants) present in the liquid phases at process conditions. The higher basicity ($\text{CaO}/\text{SiO}_2 \approx 0.8\text{--}0.9$) and fluorite percentage ($\approx 9\text{--}11$ mass%) present in samples A and B determine a low viscosity in the liquids present at lower melting temperatures than sample C. Also, these liquids (L_{1A} , L_{2A} and L_{1B}) have lower surface tensions than those liquids predicted in powder C (L_{1C} and L_{2C}). Thus, low viscosity liquids facilitate the transport of bubbles and ions mobility in the molten slag. According to Zhang et al. [16], the decrease of the viscosity increases both the growth of bubbles and the transport of gaseous species from the melt to the bubble/slag (gas/liquid) interface. In the same way, the surface tension of molten

slags also plays an important role to determine the growth of the bubbles. In this case, a low surface tension of the melt promotes that bubbles became spherical and growth [6]. Higher size of bubbles increases fluorine gas species emissions.

It is relevant to comment that the correlation of differential thermal analysis (DTA–TG) results with HSM measurements and thermodynamic simulation allow to understand the complex casting powders systems. This type of tests is applied also for other glass systems as is described in [17, 18].

Conclusions

Three casting powders with different percentages of CaF_2 were monitored by DTA/TG. The emissions of different fluorine-species were associated with both the viscosity and the surface tension of liquids present at the emission temperatures. Thermodynamic simulations permitted to complete the complex phenomenon associated with the emissions of fluorine gases in these materials.

Casting powders containing CaF_2 produced different types of fluorine gases according to the particular chemical composition. From thermodynamic simulations, the main gaseous phases were: NaF , KF , $(\text{NaF})_2$, NaAlF_4 , KAlF_4 and SiF_4 .

Fluoride gas emissions occur at temperatures in which the systems contain one or more liquids. The composition of liquids affects the viscosity (lower viscosity was associated with higher emissions of gases). On the other hand, the type and content of surfactant affect the surface tension (lower surface tension was associated with higher emissions).

Acknowledgements The authors wish to thank Universidad Tecnológica Nacional (Argentina) for the financial support provided to this project.

References

- Brandaleze E, Di Gresia G, Santini L, Martín A, Benavidez E. Mould fluxes in the steel continuous casting process. In: Srinivasan M, editor. Science and technology of casting processes. Rijeka: InTech; 2012. p. 205–33.
- Persson M, Sheetharaman S, Seetharaman S. Kinetic study of fluoride evaporation from slags. *ISIJ Int.* 2007;47:1711–7.
- Zhou L, Wang W, Zhou K. Viscosity and crystallization behavior of F-free mold flux for casting medium carbon steels. *ISIJ Int.* 2015;55:1916–24.
- Van Ende MA, Jung IH. Development of a thermodynamic database for mold flux and application to the continuous casting process. *ISIJ Int.* 2014;54:489–95.

5. Sasaki Y, Urata H, Ishii K. Structural analysis of molten Na_2O – NaF – SiO_2 system by Raman spectroscopy and molecular dynamics simulation. *ISIJ Int.* 2003;43:1897–903.
6. Tian Y, Shuguang G, Shibing S. Effect of Al_2O_3 on surface tension of the SiO_2 – Al_2O_3 – RO – R_2O glass system. *Key Eng Mater.* 2014;633:322–5.
7. Wang L, Zhang J, Sasaki Y, Otrovski O, Zhang C. Stability of fluorine-free CaO – SiO_2 – Al_2O_3 – B_2O_3 – Na_2O mold fluxes. *Metall Mater Trans B.* 2017;2:322–5.
8. Mills K. The estimation of slag properties. Short Course. Southern African Pyrometallurgy 2011. Department of Materials, Imperial College. 2011.
9. Yung HI. Overview of the applications of thermodynamic databases to steelmaking process. *CALPHAD Comput Coupling Phase Diagr Thermochem.* 2010;34:332–62.
10. Bale CW, et al. FactSage thermochemical software and databases 2010–2016. *CALPHAD Comput Coupling Phase Diagr Thermochem.* 2016;54:35–53.
11. Cardarelli F. *Materials handbook*. 2nd ed. Berlin: Springer; 2008. p. 1110–7.
12. Mills KC, Karagadde S, Lee PD, Yuan L, Shahbazian F. Calculation of physical properties for use in models of continuous casting process-part 1: mould slags. *ISIJ Int.* 2016;56:264–73.
13. Saleem S, Vynnický M, Fredriksson H. The influence of peritectic reaction/transformation on crack susceptibility in the continuous casting of steels. *Metall Mater Trans B.* 2017;48B:1625–35.
14. Mizuno H, Esaka H, Shinozuka K, Tamura M. Analysis of the crystallization of mold flux for continuous casting of steel. *ISIJ Int.* 2008;48:277–85.
15. Zhou L, Wang W, Wey J, Zhou K. Melting and heat transfer behavior of fluorine-free mold fluxes for casting medium carbon steels. *ISIJ Int.* 2015;55:821–9.
16. Zhang ZT, Sridhar S, Cho JW. An investigation of the evaporation of B_2O_3 and Na_2O in F-free mold slags. *ISIJ Int.* 2011;51:80–7.
17. Sinouh H, Bih L, Manoun B, Lazor P. Thermal analysis and crystallization of the glasses inside the BaO – SrO – TiO_2 – NaPO_3 system. *J Therm Anal Calorim.* 2017;128:883–90.
18. Praveen J, Danewalia SS, Singh K. Influence of thermal stability on dielectric properties of SiO_2 – K_2O – CaO – MgO glasses. *J Therm Anal Calorim.* 2017;128:745–54.